

Phase-Aligned Spectral Filtering for Decomposing Spatiotemporal Dynamics

Lu Meng Tian Zheng

Department of Statistics
Columbia University

January 14, 2022

Abstract

Spatiotemporal dynamics is central to a wide range of applications from climatology, computer vision to neural sciences. From temporal observations taken on a high-dimensional vector of spatial locations, we seek to derive knowledge about such dynamics via data assimilation and modeling. It is assumed that the observed spatiotemporal data represent superimposed lower-rank smooth oscillations and movements from a generative dynamic system, mixed with higher-rank random noises. Separating the signals from noises is essential for us to visualize, model and understand these lower-rank dynamic systems. It is also often the case that such a lower-rank dynamic system have multiple independent components, corresponding to different trends or functionalities of the system under study. In this paper, we present a novel filtering framework for identifying lower-rank dynamics and its components embedded in a high dimensional spatiotemporal system. It is based on an approach of structural decomposition and phase-aligned construction in the frequency domain. In both our simulated examples and real data applications, we illustrate that the proposed method is able to separate and identify meaningful lower-rank movements, while existing methods fail.

Keywords: spatiotemporal data; dimension reduction; multivariate time series; Fourier transform; principal component series.

1 Introduction

The assimilation of spatiotemporal data is critical to the scientific discovery in a wide range of fields such as environmental sciences where temporal data are collected by spatially distributed remote-sensing platforms and sensor networks, and neural sciences where time series of brain activities are measured using images from

functional Magnetic Resonance Imaging (fMRI) or electroencephalography (EEG) signals. Most such analyses are descriptive. In other words, they employ statistical models that would shed lights on the spatially dependent evolving processes of interests. Currently, there are two main approaches of spatiotemporal modeling (see [1] for an overview): i) via joint space-time covariance functions [2; 3; 4; 5; 6; 7; 8; 9; 10; 11]; ii) via direct dynamic models that uses either time-varying spatial models or spatially structured multivariate time series models [12; 13; 14; 15; 16; 17; 18; 19]. The latter is often preferred in practice since it represents, comparing to the former, a more direct systems-oriented approach in connection with the scientific context concerning the spatiotemporal processes of interest. It can also be more flexibly integrated with stochastic methods and dynamic programming algorithms.

Current technologies have enabled faster and denser data collection in both time and space. A major challenge in the analysis of today’s spatiotemporal data is their high dimensionality. On the other hand, it is believed that the true spatiotemporal system being measured is smooth in space and time, rendering a lower-rank underpinning dependence structure for the high-dimensional observations. Identification of this lower-rank structure will therefore lead to scientific insights. Furthermore, in applications that involve predictive modeling using high-dimensional spatiotemporal data, information-preserving dimension reduction is of utmost importance to the construction of a reliable predictor.

Existing dimension reduction methods for independent observations largely fall into two categories. *variable selection* methods (e.g., via regularization as in LASSO [20]) that reduce the dimension of the original variable space by selecting a subset of the most “important” variables. *Filtering* or *transformation* methods (e.g. factor analysis [21], Kalman filter [22], independent component analysis [23] and *etc.*), on the other hand, identify a low-dimensional manifold (i.e., a transformed feature space) that carries a substantial amount of the original information. Principal component analysis (PCA) [24] is one of the most popular tools for dimension reduction via transformation (see [25] for examples). It is also known as Hotelling transform [26], discrete Karhunen-Loève transform (KLT) [27; 28], and empirical orthogonal functions (EOF) [29]. PCA explores the covariance structure among the elements of a multivariate random vector and performs linear transformations such that the transformed variables, which are called principal components, are linearly uncorrelated and carry a maximal amount of original information. In most applications, a small number of leading components with the highest variances preserve a large portion of the overall variability in the original multivariate random vector.

For temporal observations on a high-dimensional vector of spatial locations, however, the aforementioned methods for independent observations fail to account for temporal dependence that is possibly coupled with spatial dependence. For example, by treating observations at different time points as independent, principal components can be derived from spatiotemporal data. These principal components are contemporaneously uncorrelated but will exhibit autocorrelation and cross-autocorrelation

at different time lags, which are hard to interpret and model. As a result, one can find a long list of filtering methods in the literature that are specifically designed for multivariate time series analysis [30; 31; 32; 33; 34; 35; 36; 37; 38]. In particular, the generalized dynamic factor model proposed by [33] decomposes the original multivariate process into moving averages of orthonormal white noises of a lower dimension. However, the model was not intended to provide a structural interpretation [33]. The singular spectral analysis by [39] decomposes the higher-dimensional series into additive components presenting trend, seasonal component and noise respectively. Matteson and Tsay (2011) [35] directly looked for a contemporaneous linear transformation so that the transformed variables, which they call dynamic orthogonal principal components, have no linear and quadratic cross-correlation over time. Chang *et al.* (2014) [37] also searched for a contemporaneous linear transformation so that the transformed multivariate time series form a group structure where any pair of transformed series from different groups will exhibit no cross-correlation. Neither [35] or [37] considered possible lags between original variables and the latent factors. Furthermore, the targeted transformations are not guaranteed to exist. None of these methods can discover interpretable spatially evolving dynamic components, as we will show using extensive simulations.

To address the dimension reduction and signal decomposition problem for multivariate time series, [40] proposes a spectral approach that directly decompose the spectral density matrices in the frequency domain and construct two sets of linear filters based on selected eigenvectors. The first set of filters transform the original high-dimensional series to low-dimensional *principal component series* with zero coherence among each other. The second set transforms the principal component series back to a lower-rank component of the original data. It leads to the most efficient dimension reduction for multivariate time series in terms of minimum mean squared error. Despite its elegant mathematical rigor, it has not been widely used in practice due to the lack of interpretability of the filtered principal component series and components. In particular, it is not clear how one should select eigenvectors at different frequencies to assemble interpretable filtered components. In terms of spatiotemporal data, for example, an interpretable component should be an oscillating dynamics in the space, which could correspond to different energy level and loadings (eigenvectors) at different frequencies. Therefore, using the eigenvector corresponding to the k -th largest eigenvalue at every frequency, as suggested in [40], to assemble filters is not well motivated.

In this paper, we show that a number of spatial dynamic systems such as *phase propagation* result in a spatially-structured signature in the *complex argument* (or *phase offset*) of their *Fourier transform*, which is preserved across frequencies up to a linear transformation. Taking advantage of this result, we propose a spatial phase-aligned algorithm for constructing phase-aligned spectral filters, adapting the spectral approach of [40] to spatiotemporal data (Figure 1). Eigenvectors from different frequencies in the *frequency domain* are clustered based on their complex argument to

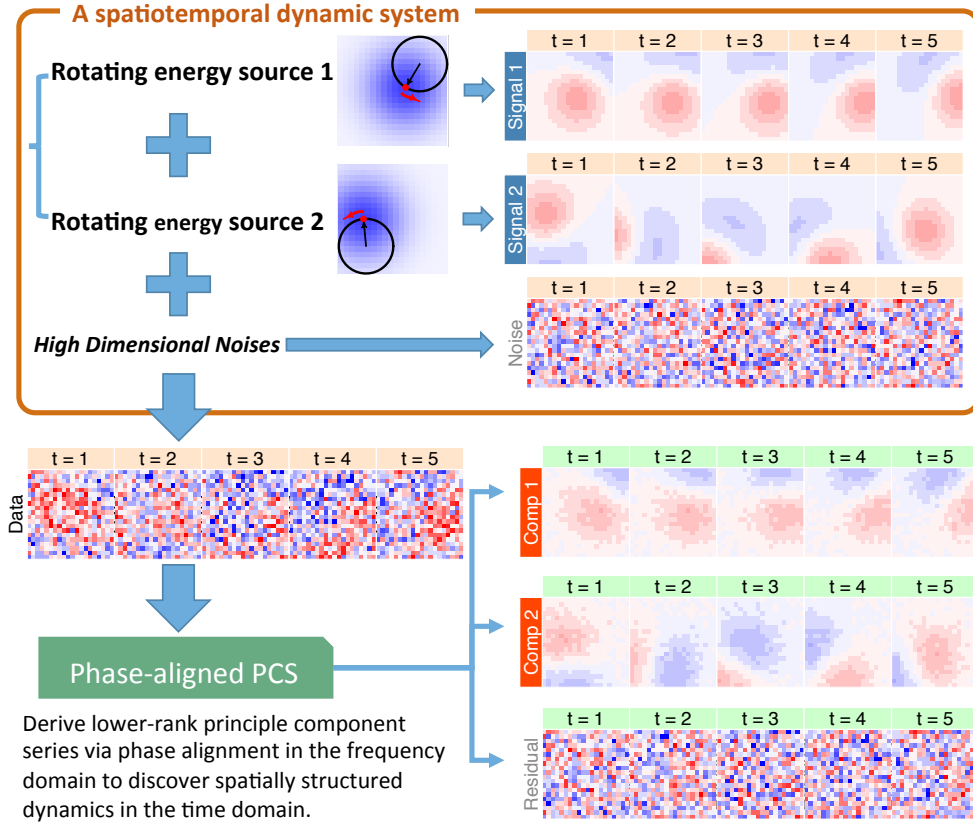


Figure 1: The proposed phase-aligned spectral filtering method discovers individual dynamic components from spatiotemporal data that consist of lower-rank smooth dynamic signals and high-dimensional noises.

create filters that deliver interpretable spatial dynamics in the *time domain*. In both simulations and empirical applications, the proposed phase-aligned spectral filtering method returns clean and interpretable lower-rank spatiotemporal dynamics that explain a substantial proportion of the observed data.

2 Methodology

2.1 Phase-aligned spectral filtering: an outline.

Our proposed *phase-aligned spectral filtering* method have two main motivations. The first motivation is Brillinger’s dimension reduction strategy for multivariate time series using eigenvalue decomposition applied on the spectral density matrices in the frequency domain [40]. By assembling linear filters based on eigenvectors from different frequencies, we can derive principal component series (PCS) that have zero coherence at all frequencies. This is a desirable properties for further predictive mod-

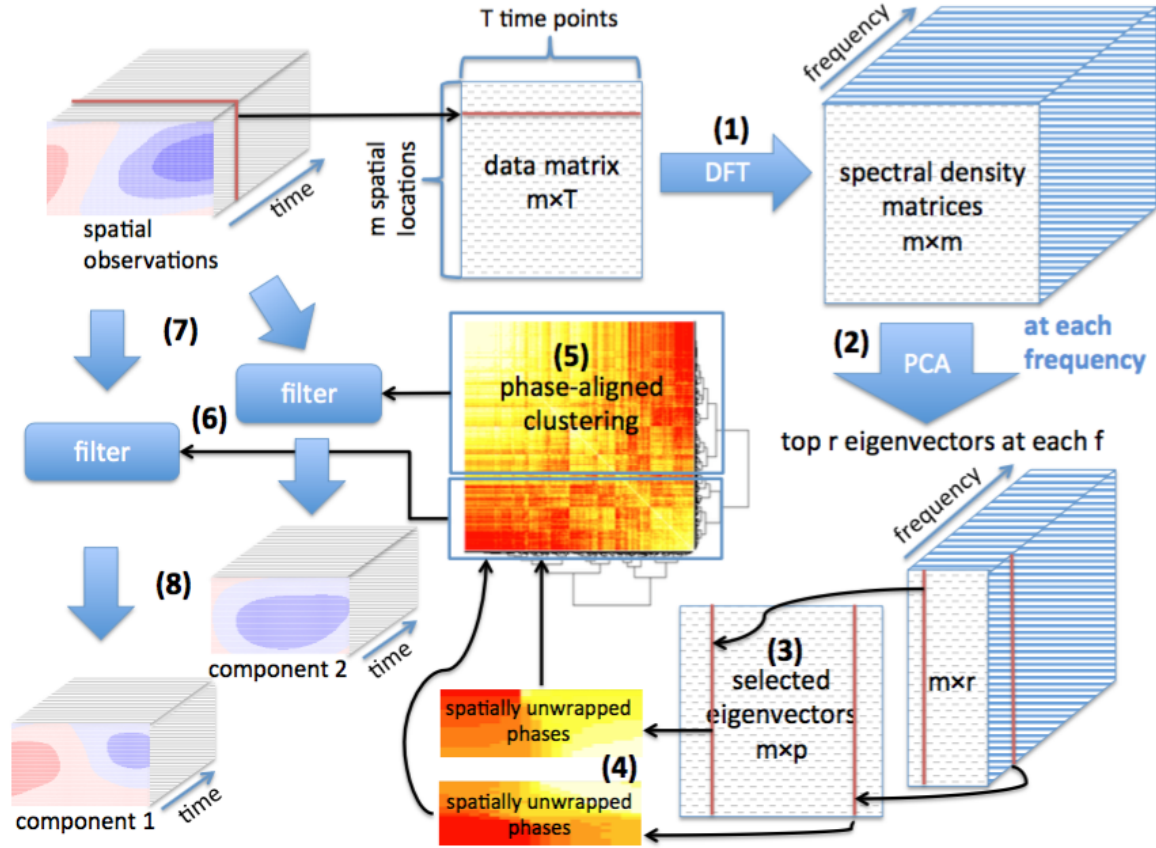


Figure 2: Outline of the phase-aligned spectral filtering decomposition of spatiotemporal dynamics. From vectorized spatial observations over time, we first apply (1) discrete Fourier transform (DFT) to derive spectral density matrices. Applying (2) principal component analysis at each frequency, we select eigenvectors corresponding to the top r eigenvalues. We further impose (3) shrinkage on the selected eigenvectors to remove those corresponding to eigenvalues below a predetermined threshold. Raw phase-values of selected eigenvectors are then (4) unwrapped spatially and then (5) clustered. A pair of linear filters based on eigenvectors in a cluster were (6) constructed. Filtering the originally observed spatiotemporal data via two consecutive steps (7) and (8), we derive separated low-rank spatially smooth dynamic components of the observed system. More details on these steps can be found in Section 2.5.

eling using such series. To maintain the maximal information in the original series while reducing dimensions, eigenvectors corresponding to top eigenvalues are selected from each frequency. Applying a second set of filters constructed using the conjugate of of these selected eigenvectors at different frequencies, the principal component series can be filtered back into lower-rank components of the original data. In [40], it is suggested that the k th eigenvector from each frequency be used to assemble the filters for the k th component. However, this is not well motivated nor required for having zero coherence among the PCS or the rest of Brillinger’s results in [40]. As our second motivation, in this paper, we identify a link between phase-correlation in spectral densities and a number of low-rank smooth spatiotemporal dynamics. This provides a novel approach for assembling spectral filters that will decompose the original high-dimensional time series into lower-rank spatially smooth dynamic components. The proposed framework follow a sequence of steps as shown in Figure 2.

In the following sections, we explain in details the phase-aligned spectral filtering method, starting with dimension reduction in the frequency domain (Section 2.2), eigenvalue shrinkage (Section 2.3) and reassembling of principle component series (Section 2.4). Section 2.5 explains the computational steps of decomposing a high-dimensional spatiotemporal data set using the proposed phase-aligned spectral filtering method.

2.2 Dimension reduction in the frequency domain

Consider a real-valued spatiotemporal process $\{Z_{s,t} \in \mathbb{R} : s \in \mathcal{D}_m, t \in \mathcal{T}\}$ where the discrete spatial domain $\mathcal{D}_m = \{s_1, \dots, s_m\} \subset \mathcal{D}$ contains a set of m locations and $\mathcal{T} = \{0, \pm 1, \pm 2, \dots\}$. Assume that $\mathbf{Z}_t = \{Z_{s,t} : s \in \mathcal{D}_m\}$ is a second-order stationary m -dimensional vector-valued time series with mean $\boldsymbol{\mu}$ and $m \times m$ spectral density $f_{zz}(\omega)$ for $\omega \in [-\frac{1}{2}, \frac{1}{2}]$. Without loss of generality, we assume $\boldsymbol{\mu} = \mathbf{0}$. The spectral density matrix $f_{zz}(\omega)$ is a complex-valued positive semidefinite Hermitian matrix in the form of

$$f_{zz}(\omega) = \sum_{h=-\infty}^{\infty} \Gamma(h) e^{-2\pi i \omega h}, \quad (1)$$

where $\Gamma(h)$ is the autocovariance function of \mathbf{Z}_t .

Brillinger (1981)[40] stated that for each integer $1 \leq r \leq m$, there exist a pair of filters $\{\mathbf{C}_\tau^{[r]} \in \mathbb{R}^{r \times m} : u \in \mathcal{T}\}$ and $\{\mathbf{B}_\tau^{[r]} \in \mathbb{R}^{m \times r} : u \in \mathcal{T}\}$ that minimizes the mean squared error

$$\mathbb{E}(\mathbf{Z}_t - \tilde{\mathbf{Z}}_t)^\top (\mathbf{Z}_t - \tilde{\mathbf{Z}}_t) \quad (2)$$

where

$$\mathbf{X}_t^{[r]} = \sum_{\tau=-\infty}^{\infty} \mathbf{C}_{t-\tau}^{[r]} \mathbf{Z}_\tau, \text{ and, } \tilde{\mathbf{Z}}_t = \sum_{\tau=-\infty}^{\infty} \mathbf{B}_{t-\tau}^{[r]} \mathbf{X}_\tau^{[r]}. \quad (3)$$

The sequence of matrices are

$$\mathbf{C}_\tau^{[r]} = \int_{-1/2}^{1/2} \mathbf{C}^{[r]}(\omega) \exp(2\pi i\tau\omega) d\omega, \quad (4)$$

$$\mathbf{B}_\tau^{[r]} = \int_{-1/2}^{1/2} \mathbf{B}^{[r]}(\omega) \exp(2\pi i\tau\omega) d\omega, \quad (5)$$

where

$$\mathbf{C}^{[r]}(\omega) \begin{pmatrix} \overline{\mathbf{v}_{(1)}(\omega)^\top} \\ \vdots \\ \overline{\mathbf{v}_{(r)}(\omega)^\top} \end{pmatrix}, \quad \mathbf{B}^{[r]}(\omega) (\mathbf{v}_{(1)}(\omega), \dots, \mathbf{v}_{(r)}(\omega)) = \overline{\mathbf{C}^{[r]}(\omega)^\top},$$

and $\mathbf{v}_{(1)}(\omega), \dots, \mathbf{v}_{(r)}(\omega)$ are the r eigenvectors of $f_{zz}(\omega)$ corresponding to its first r largest eigenvalues $\lambda_{(1)}(\omega), \dots, \lambda_{(r)}(\omega)$. The resulted $\mathbf{X}_t^{[r]}$, referred to as principal component series, has a spectral density matrix

$$f_{xx}(\omega) = \begin{pmatrix} \lambda_{(1)}(\omega) & & \mathbf{0} \\ & \ddots & \\ \mathbf{0} & & \lambda_{(r)}(\omega) \end{pmatrix}, \quad (6)$$

which means any pair of the principal component series $X_{k,t}$ and $X_{j,t}$ for $k \neq j$ has zero coherence.

2.3 Further dimensionality reduction by shrinkage

At each frequency, we decompose the spectral density as follows

$$\begin{aligned} f_{zz}(\omega) &= \sum_{j=1}^m \lambda_{(j)}(\omega) \mathbf{v}_{(j)}(\omega) \overline{\mathbf{v}_{(j)}(\omega)^\top} \\ &= \sum_{j=1}^r \lambda_{(j)}(\omega) \mathbf{v}_{(j)}(\omega) \overline{\mathbf{v}_{(j)}(\omega)^\top} \\ &\quad + \sum_{j=r+1}^m \lambda_{(j)}(\omega) \mathbf{v}_{(j)}(\omega) \overline{\mathbf{v}_{(j)}(\omega)^\top} \\ &= f_{\tilde{z}\tilde{z}}(\omega) + f_{\epsilon\epsilon}(\omega). \end{aligned}$$

where $f_{\epsilon\epsilon}(\omega)$ is the spectral density of the error series $\boldsymbol{\epsilon}_t = \mathbf{Z}_t - \tilde{\mathbf{Z}}_t$. In many cases, the spectral power concentrates in a relatively small area along the frequency axis, that is, if we pool the first r largest eigenvalues at all frequencies, there remain a large proportion of eigenvalues being relatively small, or even close to zero. Here we propose a threshold Δ and further define

$$r_\omega = \max\{j : \lambda_{(j)}(\omega) \geq \Delta\}.$$

The decomposition of the spectral density of \mathbf{Z}_t becomes

$$\begin{aligned} f_{zz}(\omega) &= \sum_{j=1}^{r_\omega} \lambda_{(j)}(\omega) \mathbf{v}_{(j)}(\omega) \overline{\mathbf{v}_{(j)}(\omega)}^\top \\ &\quad + \sum_{j=r_\omega+1}^m \lambda_{(j)}(\omega) \mathbf{v}_{(j)}(\omega) \overline{\mathbf{v}_{(j)}(\omega)}^\top \\ &\triangleq f_{\tilde{z}^* \tilde{z}^*}(\omega) + f_{\epsilon^* \epsilon^*}(\omega). \end{aligned}$$

If r_ω is 0, then $f_{\tilde{z}^* \tilde{z}^*}(\omega) = 0$. Compared to the previous filtered series $\tilde{\mathbf{Z}}_t$, the new filtered series $\tilde{\mathbf{Z}}_t^*$ is less noisy and more robust. This shrinkage step is also important and necessary in the next phase-aligned reassembling step.

2.4 Reassembling principal component series

The spectral density of the r -dimensional principal component series \mathbf{X}_t 's obtained in (3) is diagonal and aligned in descending order. However, the k -th assembled principal component series $X_{k,t}$ that is constructed using the eigenvector corresponding to the k -th largest eigenvalue at every frequency lack interpretability. As a matter of fact, given a pool of eigenvectors from different frequencies derived by previous steps, we can reassemble eigenvectors at different frequencies arbitrarily yet still maintain the zero coherence property of the resulting principal component series. The problem we are interested in solving is: given $(\mathbf{v}_{(1)}(\omega), \mathbf{v}_{(2)}(\omega), \dots, \mathbf{v}_{(r)}(\omega))$, how do we assemble principal component series from a pool of eigenvectors at different frequencies, so that to have an interpretable decomposition?

We build a solution to the above problem based on the fact that a shift in the time domain corresponds to a phase change in the frequency domain. This change is a linear function of frequency. For example, if a signal is propagating, the observations would take form as decayed and delayed versions of the original signal. Furthermore, if the rate of energy decay and the amount of time delay only depend on the location of observation and the original location of the signal, that is, does not depend on time, the corresponding phase of the Fourier transform of such signals would be perfectly correlated in the frequency domain.

Simple dynamics such as signal propagating and sensing towards mobile energy sources lead to correlated phase in the frequency domain (see proofs in the Appendix). If we cluster eigenvectors with correlated phases to assemble principle component series, the filters constructed from each cluster would produce meaningful and interpretable spatiotemporal dynamics.

2.5 Decomposition by phase-aligned spectral filtering

In this section, we will outline the steps for the phase-aligned spectral filtering method.

Parameter estimation. In practice, we only have observations on a finite time horizon. Let $\{z_{s,t} \in \mathbb{R} : s \in \mathcal{D}_m, t \in \mathcal{T}_n\}$ denote the observed data where $\mathcal{T}_n = \{1, \dots, n\} \subset \mathcal{T}$. In order to assemble the desired phase-aligned spectral filters as described above, we need to estimate the paired filters $\{\mathbf{C}_\tau = (\mathbf{C}_{1,\tau}^\top, \dots, \mathbf{C}_{r,\tau}^\top)^\top \in \mathbb{R}^{r \times m}\}$ and $\{\mathbf{B}_\tau = (\mathbf{B}_{1,\tau}, \dots, \mathbf{B}_{r,\tau}) \in \mathbb{R}^{m \times r}\}$ from this finite sample so that the principal component series

$$\mathbf{x}_{k,t} = \sum_{\tau=1}^n \mathbf{C}_{k,t-\tau} \mathbf{z}_\tau$$

has diagonal or approximately diagonal spectral density and its resulting dynamic component $\tilde{\mathbf{z}}_t^{(k)}$ obtained from

$$\tilde{\mathbf{z}}_t^{(k)} = \sum_{\tau=1}^n \mathbf{B}_{k,t-\tau} \mathbf{x}_{k,\tau}$$

has correlated phases across frequencies where $1 \leq k \leq r$, $\mathbf{C}_{k,\tau}$ is the k -th row vector of \mathbf{C}_τ and $\mathbf{B}_{k,\tau}$ is the k -th column vector of \mathbf{B}_τ .

The paired filters are constructed from the eigenvectors of spectral density matrices $f_{zz}(\omega)$. We estimate the eigenvectors $\mathbf{v}_j(\omega)$ by the eigenvectors of estimated spectral density $\hat{f}_{zz}(\omega)$. The spectral density matrices at Fourier frequencies $\omega_j = j/n$ for $j = 0, \dots, n-1$ are estimated by the smoothed periodogram

$$\hat{f}_{zz}(\omega_j) = \sum_{k=-q}^q h_k P(\omega_j + \frac{k}{n}),$$

where $P(\omega_j)$ is the raw periodogram and h_k is a smoothing kernel of bandwidth equal to $(2q+1)$ satisfying: i) $h_k > 0$; ii) $\sum_{k=-q}^q h_k = 1$; and iii) $q \rightarrow \infty$ and $q/n \rightarrow 0$, $\sum_{k=-q}^q h_k^2 \rightarrow 0$ as $n \rightarrow \infty$.

Phase unwrapping. We obtain the raw phase of the estimated k th eigenvector, $\text{Arg}(\hat{\mathbf{v}}_k(\omega_j))$ at frequency ω_j , by taking logarithm of the estimated eigenvector $\hat{\mathbf{v}}_k(\omega_j)$ and extract the imaginary part. However, the resulting phase estimate is only given as the actual phase modulo 2π , between $-\pi$ and π . Even when the phase vectors of two eigenvectors are completely correlated, such a loss of information will render them much less correlated. In order to carry out our phase-aligned reassembling of eigenvectors, we need to recover the true phase up to a linear transformation.

The computed raw phase (modulo 2π) has discontinuities near π and $-\pi$. We assume the true phase is continuous in space. Based on this assumption, we can then unwrap the raw phase values, in other words, resolve the jumps of phase values in a two dimensional space to derive continuous phase values. Over the spatial locations $s_k \in \mathbb{R}^2$, we apply the two-dimensional phase unwrapping algorithm proposed in [41] to each $\text{Arg}(\hat{\mathbf{v}}_k(\omega))$ for $k = 1, \dots, r_\omega$. The algorithm changes the raw values of $\text{Arg}(\mathbf{v}_k(\omega_j))$ by adding $2c\pi$ with $c \in \mathbb{Z}$ at jumps so that the unwrapped phase values, denoted by $\widetilde{\text{Arg}}(\hat{\mathbf{v}}_k(\omega_j))$ attain a maximum level of continuity over spatial locations.

Phase clustering. On the unwrapped phases $\widetilde{\text{Arg}}(\hat{\mathbf{v}}_k(\omega_j))$ of the selected eigenvectors whose eigenvalues $\hat{\lambda}_k(\omega_j)$ are greater than or equal to Δ , we deploy hierarchical clustering as the clustering algorithm with one minus correlation as the distance measure and Ward's clustering criterion [42] as the linkage agglomeration method.

We then construct filters from each cluster to create reassembled principal component series that correspond to dynamics with correlated phases in their spectral densities. To construct the desired filters from each cluster, we label each of the selected eigenvector by its group number from the unwrapped phase clustering results. And then the paired filters for the k -th principal component series and its corresponding dynamic component are constructed by

$$\hat{\mathbf{C}}_{k,\tau} = \frac{1}{n} \sum_{j=0}^{n-1} \overline{\hat{\mathbf{v}}_k(\omega_j)}^\top \mathbb{1}_{\hat{\lambda}_k(\omega_j) \geq \Delta} \exp(2\pi i \tau \omega_j), \quad (7)$$

$$\hat{\mathbf{B}}_{k,\tau} = \frac{1}{n} \sum_{j=0}^{n-1} \hat{\mathbf{v}}_k(\omega_j) \mathbb{1}_{\hat{\lambda}_k(\omega_j) \geq \Delta} \exp(2\pi i \tau \omega_j), \quad (8)$$

where $\hat{\mathbf{v}}_k(\omega_j)$ is the eigenvector with a group label equal to k when its eigenvalue $\hat{\lambda}_k(\omega_j)$ is greater than or equal to Δ .

The phase-aligned spectral filtering algorithm. The complete phase-aligned spectral filtering decomposition procedure for spatiotemporal dynamics is summarized in Algorithm 1. The step numbers are the same as in Figure 2.

Algorithm 1: Phase-aligned spectral filtering decomposition

Input: Data $\{z_{s,t} : s \in \mathcal{D}_m, t \in \mathcal{T}_n\}$, number of top eigenvalues considered r and threshold Δ

Output: dynamic components $\{\tilde{z}_{s,t}^{(k)} : s \in \mathcal{D}_m, t \in \mathcal{T}_n, k = 1, \dots, r\}$

- 1 Estimate the spectral density $f_{zz}(\omega_j)$ for $\omega_j = j/n$ with $j = 0, \dots, n-1$;
 - 2 Calculate the top r eigenvalues and eigenvectors for each $f_{zz}(\omega_j)$;
 - 3 Shrink the eigenvalues by the threshold Δ and obtain the corresponding eigenvectors;
 - 4 Unwrap the phases of the selected eigenvectors;
 - 5 Cluster the selected eigenvectors using one minus the correlations of their unwrapped phases as dissimilarity;
 - 6 Construct paired filters from each cluster;
 - 7 Apply each of the \mathbf{C} filters to the data $z_{s_1:s_m, 1:n}$ and obtain the reassembled principal component series;
 - 8 Apply each of the \mathbf{B} filters to its corresponding principal component series and get the phase-aligned dynamic component.
-

3 Simulation results

We first illustrate the proposed phase-aligned spectral filtering method using multiple constructed low-dimensional dynamic systems in an area where observations of the entire system are taken on a 20×20 grid of spatial locations: on $\mathcal{D} = [0, 20]^2 \subset \mathbb{R}^2$ with grid blocks $\{s_{j,k} = [j-1, j] \times [k-1, k] \subset \mathbb{R}^2 : 1 \leq j \leq 20, 1 \leq k \leq 20, j \in \mathbb{N}, k \in \mathbb{N}\}$ and grid locations being the centers of the corresponding grid blocks. The phase-aligned spectral filtering method is then compared with a number of comparison methods found in the literature.

3.1 Scenario I: rotating energy sources

In this example, we create a scenario where the observed value at a given grid location and a given time point is the total energy absorbed by the unit block area centered at this given grid location, from all rotating energy sources.

On the 20×20 grid, there are two energy sources affecting the area, each of which moves following a circular trajectory. The two trajectories are centered at $c_c^{(1)} = (15, 15)$ and $c_c^{(2)} = (5, 5)$ respectively, with radius of $r_c^{(1)} = r_c^{(2)} = 5$. The two energy sources move different angular velocities of $v_\theta^{(1)} = 2\pi/20$ and $v_\theta^{(2)} = 2\pi/5$ per time unit counterclockwise respectively. The initial positions of the two energy sources on the trajectory circles, denoted by $\theta_0^{(1)}$ and $\theta_0^{(2)}$ measuring the angular distance from the horizontal axis. They are randomly assigned in each simulation. The i -th energy source's position at $t = 0$ can therefore be written as $c_c^{(i)} + (r_c^{(i)} \cos \theta_0^{(i)}, r_c^{(i)} \sin \theta_0^{(i)})$ with $\theta_0^{(i)}$ uniformly sampled between 0 to 2π for $i = 1, 2$. At any subsequent time point t , the i -th energy source's position is

$$c_t^{(i)} = \begin{pmatrix} c_{t,1}^{(i)} \\ c_{t,2}^{(i)} \end{pmatrix} = c_c^{(i)} + \begin{pmatrix} r_c^{(i)} \cos(\theta_0^{(i)} + v_\theta^{(i)} t) \\ r_c^{(i)} \sin(\theta_0^{(i)} + v_\theta^{(i)} t) \end{pmatrix}, \quad i = 1, 2.$$

Assume that the energy absorbed from the energy source decays exponentially in squared distance. For $s \in \mathcal{D}, t \in \mathcal{T}_n = \{1, 2, \dots, n\}$, we can explicitly write down the energy at location s and time t absorbed from the i -th energy sources positioned at $c_t^{(i)}$ as

$$E_{s,t}^{(i)} = E_0^{(i)} \exp\left(-\frac{\|s - c_t^{(i)}\|^2}{\gamma^{(i)}}\right)$$

where $E_0^{(i)}$ is the total emitted energy of the i -th energy source during any unit time. $E_0^{(i)}$ is assumed to be a constant for simplicity. The total amount of energy measured at location s and time t is the sum of energy absorbed from all sources, that is,

$$E_{s,t} = \sum_{i=1}^2 E_{s,t}^{(i)} = \sum_{i=1}^2 E_0^{(i)} \exp\left(-\frac{\|s - c_t^{(i)}\|^2}{\gamma^{(i)}}\right).$$

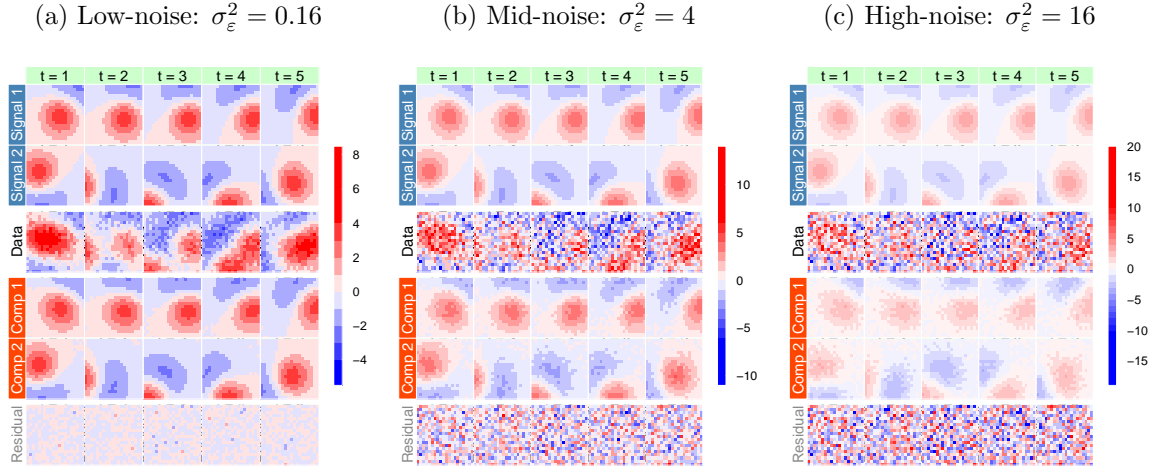


Figure 3: Phase-aligned dynamic decomposition in the two-rotating-energy-source simulation from $t = 1$ to $t = 5$ in the low-, mid- and high-noise level settings.

Thus, the amount of energy the grid block $s_{j,k}$ absorbs at time t is

$$z_{(j,k),t} = \int_{s \in s_{j,k}} E_{s,t} ds.$$

The total emitted energy $E_0^{(i)}$ is set to be 1000 and the bandwidth parameter $\gamma^{(i)}$ is set to be 5 for $i = 1, 2$. We use the demeaned $\mathbf{z}_t^{(1)}$ and $\mathbf{z}_t^{(2)}$ as the underlying dynamic systems that affect the grid area. The final observed measurements are the energy distributed by these two rotating sources overlaid and superimposed on each other with high dimensional white noises added, i.e.,

$$\mathbf{y}_{(j,k),t} = z_{(j,k),t} + \varepsilon_{(j,k),t}, \quad 1 \leq j \leq 20, 1 \leq k \leq 20.$$

Using vectorized notation for $\varepsilon_{(j,k),t}$, we define $\boldsymbol{\varepsilon}_t = (\varepsilon_{1,t}, \varepsilon_{2,t}, \dots, \varepsilon_{400,t})^\top$. We assume that $\boldsymbol{\varepsilon}_t \sim \mathcal{N}(0, \sigma_\varepsilon^2 \mathbf{I}_m)$ where $m = 400$. We set three noise levels in this simulated scenario: low-noise level with $\sigma_\varepsilon^2 = 0.16$, mid-noise level with $\sigma_\varepsilon^2 = 4$ and high-noise level with $\sigma_\varepsilon^2 = 16$. The top three rows of Fig. 3 are the level plots of the two rotating energy sources $\mathbf{z}_t^{(1)}$ and $\mathbf{z}_t^{(2)}$ along with the observed data \mathbf{y}_t from $t = 1$ to $t = 5$ under the three noise-level settings. As one can see, when σ_ε^2 increases to 16, the two dynamic systems are barely discernible in the superimposed observed data.

The performance of our phase-aligned spectral filtering (PASF) algorithm was evaluated on the simulated data under these three noise level settings. See Appendix for implementation details. The lower three rows of Fig. 3 display the decomposition results by phase-aligned spectral filtering (PASF) in the low-, mid- and high-noise level settings respectively. Rows 4 and 5 are the identified dynamic components using our proposed method. Under the low-noise setting, the first and second components

explain 48% and 47% of the variability in observed data respectively. When $\sigma_\varepsilon^2 = 4$ (mid-noise level), each of the two dynamic components accounts for 23% of the data’s variability. When σ_ε^2 increases to 16 (an overwhelmingly high noise level), variability carried by the two filtered components drops to 8%. It can be seen clearly from Fig. 3 that the phase-aligned spectral filtering (PASF) approach is still able to capture and separate the underlying dynamic systems even when the signal to noise ratio drops below 0.1 (the variance of the signals is approximately 1.6). Row 6 of each panel displays the residuals after we subtract the filtered components constructed by phase-aligned spectral filtering (PASF), which resemble white noises. See *Supplement Information* for animated plots of these simulation results.

For comparison, we also applied the principal component analysis (PCA), independent component analysis (ICA), singular spectrum analysis (SSA) [39] and principal component analysis for time series (PCA4TS) [37] to the simulated data from the *rotating energy source* example. Fig. 4 provides a side-by-side comparison of the decomposition results obtained by phase-aligned spectral filtering (PASF) and these methods found in the literature, under the low-noise level setting with $\sigma_\varepsilon^2 = 0.16$. The top left panel displays the ground truth, i.e., the true signals $\mathbf{z}_t^{(1)}$ and $\mathbf{z}_t^{(2)}$ that generate the observed data \mathbf{y}_t . The top right panel is the two components as well the residuals from our phase-aligned spectral filtering (PASF) method. The remaining panels are the resulting dynamic components and corresponding residuals computed by the literature methods (See Appendix for implementation details of these literature methods.). Comparison results under the mid- and high-noise level setting can be found in Appendix as Fig. A2 and Fig. A3.

None of the literature methods is able to recover the two underlying dynamic systems as our method does. The dynamics yielded from PCA and ICA are distant from the true dynamics since they can only capture linear features with no time dependence. SSA is able to separate the smooth dynamics from the noisy data but failed to separate them. The performance of PCA4TS is better than PCA and ICA but worse than SSA in the low-noise setting, and behaves more like PCA in the mid- and high-noise level settings.

Animated level plots of these decompositions can be found in Appendix.

3.2 Scenario II: signal propagation

The second spatiotemporal system of dynamics considered in our simulation study involves a scenario where multiple signal processes propagate on a grid. Different from the previous scenario, here the signal sources do not move. Rather, the signals propagate along preset directions. Observed value at any spatial location and at a given time t is then the sum of all propagated signals at this location and time. We further assume that the magnitude of signals decays as it propagates. Assume that four independent univariate autoregressive processes, denoted as X_k for $k = 1, 2, 3, 4$, sit at the four corners of the grid. The observed value at grid block s_j for $j =$

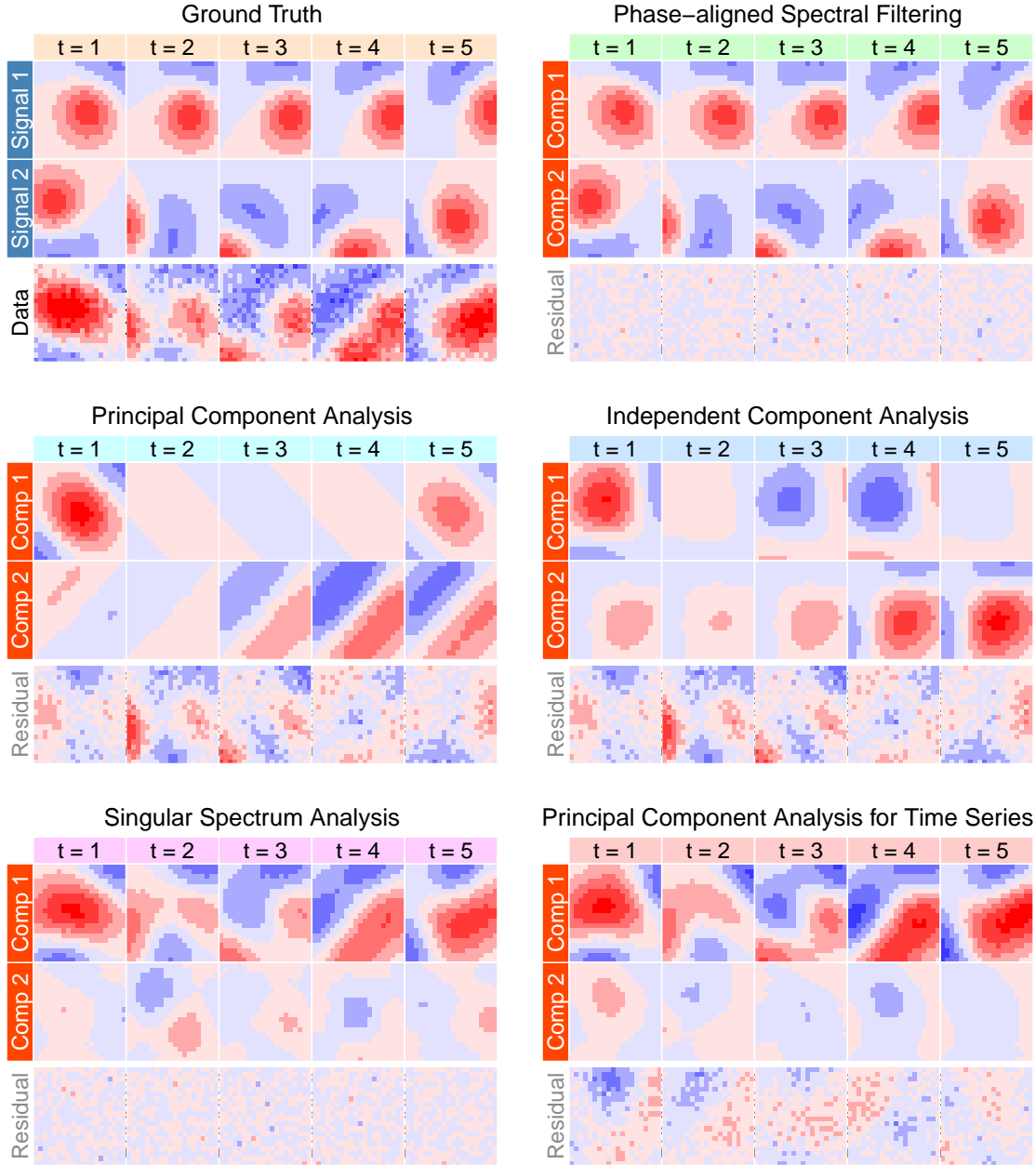


Figure 4: Decomposition results from different methods in the *two rotating energy sources* simulation example under the low-, mid- and high-noise level settings.

$1, \dots, 400$ at time t can be written as the sum of four independent signal processes with different time lags:

$$Y_{s_j,t} = \sum_{k=1}^4 a_{jk} X_{k,t-t_{jk}},$$

where $\{a_{jk}, k = 1, \dots, 4\}$ are linear weights at location s_j for the signals X_k and $\{t_{jk}, k = 1, \dots, 4\}$ are lag delays between s_j and X_k respectively. Each signal, $\{X_{k,t}\}$, $k = 1, \dots, 4$, is an autoregressive process of order 2, that is,

$$X_{k,t} = \beta_{k,1} X_{k,t-1} + \beta_{k,2} X_{k,t-2} + \varepsilon_{k,t}, \quad \varepsilon_{k,t} \sim \mathcal{N}(0, 1)$$

with $\beta_{1,1} = \beta_{2,1} = 0.9$, $\beta_{3,1} = \beta_{4,1} = -0.9$, $\beta_{1,2} = \beta_{3,2} = -0.5$, and $\beta_{2,2} = \beta_{4,2} = -0.8$.

Denote the location coordinates for $X_{k,t}$ by c_k . In our simulation, we use $c_1 = (0, 0)$, $c_2 = (20, 0)$, $c_3 = (0, 20)$ and $c_4 = (20, 20)$. For $Y_{s_j,t}$, a_{jk} and t_{jk} are decided by the spatial distance between the grid block s_j and the location of signals. Specifically,

$$a_{jk} = \exp(-\|s_j - c_k\|_2/\gamma), \quad t_{jk} = \|s_j - c_k\|_1,$$

where $\|\cdot\|_1$ and $\|\cdot\|_2$ are the L_1 and L_2 norm respectively. Parameter γ is the signals' rate of decay when propagating and is set to be 50 in this simulation. The observed value $Y_{s_j,t}$ is then the sum of four dynamic components $Y_{s_j,t}^{(1)}$, $Y_{s_j,t}^{(2)}$, $Y_{s_j,t}^{(3)}$ and $Y_{s_j,t}^{(4)}$ where

$$Y_{s_j,t}^{(k)} = e^{-\|s_j - c_k\|_2/\gamma} X_{k,t-\|s_j - c_k\|_1}, \quad k = 1, 2, 3, 4.$$

Let the vectorized notation of the propagating signal over the grid at time t be $\mathbf{Y}_t^{(k)} = (Y_{s_1,t}^{(k)}, Y_{s_2,t}^{(k)}, \dots, Y_{s_{400},t}^{(k)})^\top$. The top-left panel of Figure 5 displays the true propagating components $\mathbf{Y}_t^{(1)}$, $\mathbf{Y}_t^{(2)}$, $\mathbf{Y}_t^{(3)}$ and $\mathbf{Y}_t^{(4)}$ along with the aggregated signals as observed data. The estimated variances of the four signals are 2.55, 2.02, 1.14, and 1.09. The top-right panel of Figure 5 displays the dynamic components obtained from the proposed phase-aligned spectral filtering (PASF) method and the corresponding residuals. The corresponding components resulted from our method account for 36%, 31%, 16% and 14% of all variability in the observed data. Although the data do not display any evident patterns or dynamics, our proposed approach still manage to detect and separate the four propagating signals from the very noise-like data.

We also compare our approach with the same four literature methods that were used in the previous example. Figure 5 shows the decomposition results from these methods for comparison. The animated version of these results can be found in the Appendix. As we can see, PCA identifies the direction orthogonal to the direction of signal propagating but fails to capture the dynamics. Other literature methods capture even less than PCA. In this example, only our phase-aligned spectral filtering (PASF) method can almost fully recover the dynamic components corresponding to the four propagating signals.

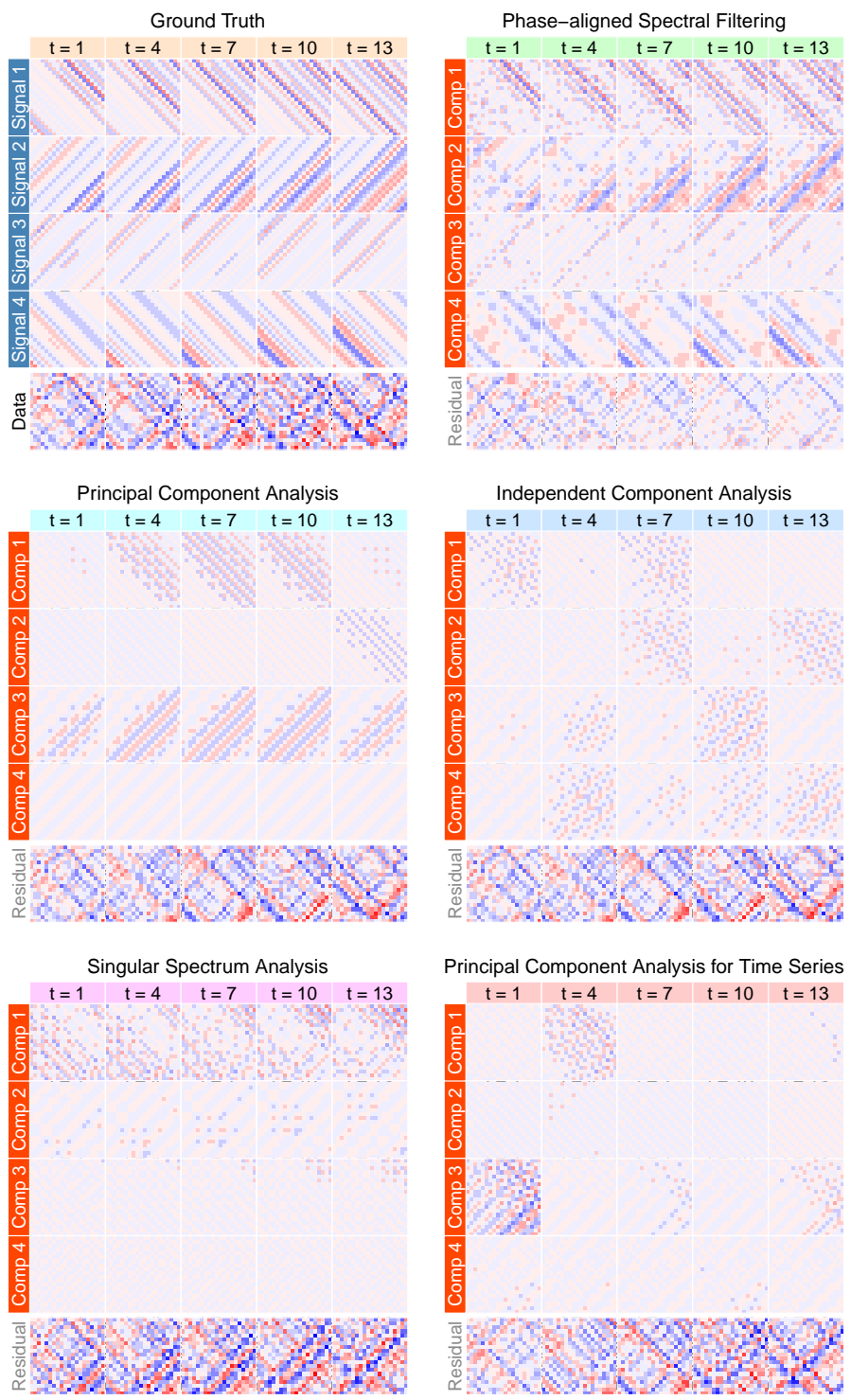


Figure 5: Decomposition results from different methods on data simulated in the four propagating signals example.

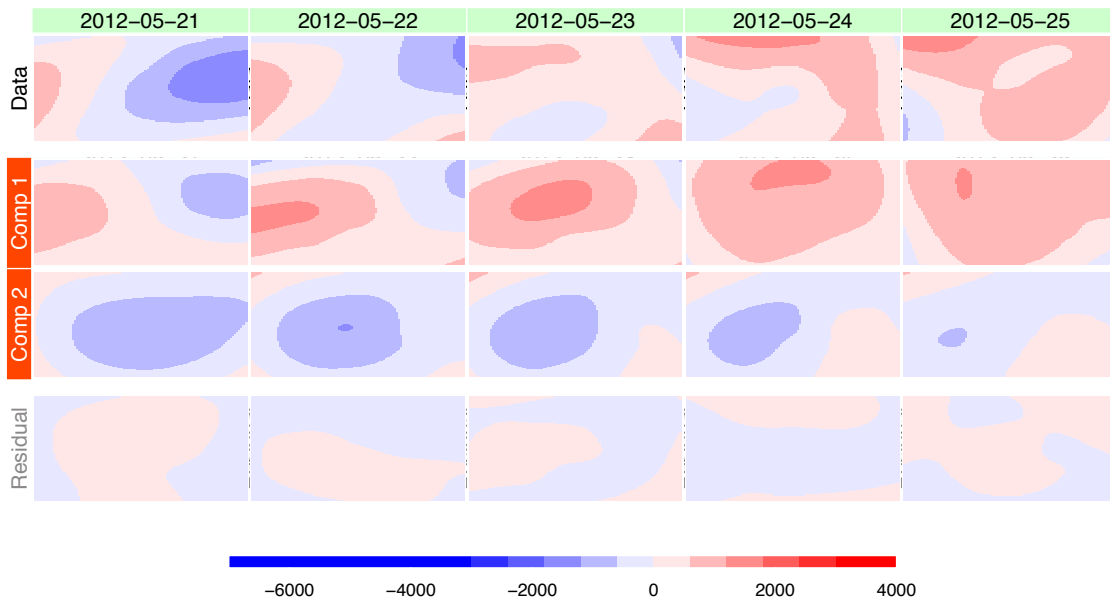


Figure 6: Phase-aligned dynamic decomposition of the sea level pressure data.

4 Real Data Analysis

The climate data analyzed in this paper is daily sea level pressure from NCEP/NCAR Reanalysis [43]. The data has a spatial resolution of 2.5° latitude \times 2.5° longitude. The grid covers a part of the pacific ocean from 30°N to 60°N and from 150°E to 230°E , which corresponds to a total of 429 spatial locations. We used observations from April 6th, 2012 to December 31, 2014, a total of 1000 time points.

Two dynamic components were identified by the proposed method. The dynamic component obtained from each cluster accounts for 63% and 32% of the total variability respectively. Figure 6 shows the two dynamic components obtained from phase-aligned spectral filtering (PASF) as well as the observed data and the residuals after spectral filtering for 5 days, May 21, 2012 to May 25, 2012. During the time range displayed in Figure 6, the first component captures a high level pressure dynamic moving from west to east and the second component captures a low level pressure dynamic moving from east to west. The animated level plots in the Appendix show similar trends throughout the entire time range. It can be seen from our decomposition results that the first component describes processes generate from the west side and propagate to the east while the second component captures processes generate from the east side and propagate to the west. These two dynamic components obtained from our approach explain a total of 95% of the information carried by the observed data.

We also applied PCA, ICA, SSA and PCA4TS to this real dataset. The resultant components from these four methods all explain about 48% of variability in the data.

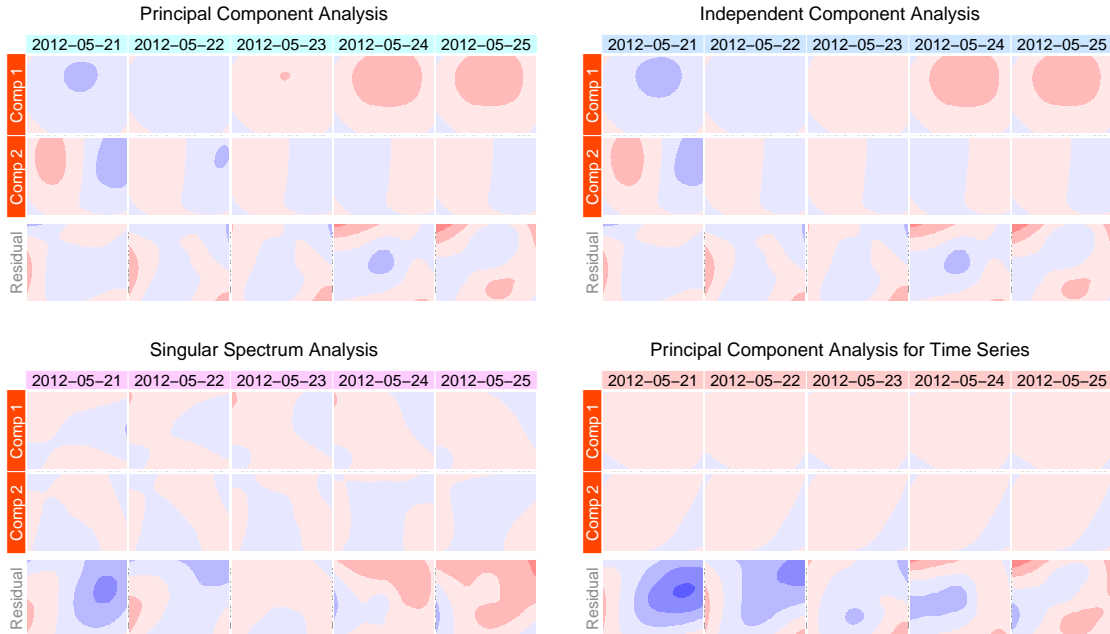


Figure 7: Decomposition results from different literature methods on the sea level pressure data.

Figure 7 shows the decomposition results as well the residuals from these literature methods from May 21, 2012 to May 25, 2012. The components are ordered by their variances. There are no evident dynamic patterns in the components extracted by these methods. Furthermore, the residuals still carry visible information and dynamics.

5 Discussion

In this paper, we propose a phase-based clustering method to create interpretable components that correspond to low-rank spatiotemporal dynamic signals with correlated phase across frequencies. In the two simulated scenarios of multiple signal sources propagating or rotating spatially, our method demonstrates excellent capabilities of capturing and separating the underlying low-dimensional dynamic systems. We also obtain interesting patterns from the components extracted using our algorithm from the analysis of sea level pressure data. The class of dynamics with phase-aligned spectral density could be very rich. Our results show that this class of dynamics include signal propagation and energy resource rotating on periodic curves (see Appendix). Although we have not fully understood its full geometric structure, our algorithm obtained clean and interpretable lower rank spatiotemporal dynamics that explains a substantial proportion of the observed data in both our simula-

tion study and analysis of climate data. Especially our approach outperforms other methods found in the literature, in terms of both information retrieval and signal separation.

References

- [1] Christopher K Wikle and Mevin B Hooten. A general science-based framework for dynamical spatio-temporal models. *Test*, 19(3):417–451, 2010.
- [2] Noel Cressie and Hsin-Cheng Huang. Classes of nonseparable, spatio-temporal stationary covariance functions. *Journal of the American Statistical Association*, 94(448):1330–1339, 1999.
- [3] Tilmann Gneiting. Nonseparable, stationary covariance functions for space–time data. *Journal of the American Statistical Association*, 97(458):590–600, 2002.
- [4] Chunsheng Ma. Families of spatio-temporal stationary covariance models. *Journal of Statistical Planning and Inference*, 116(2):489–501, 2003.
- [5] Christopher K Wikle. Hierarchical bayesian models for predicting the spread of ecological processes. *Ecology*, 84(6):1382–1394, 2003.
- [6] Michael L Stein. Space–time covariance functions. *Journal of the American Statistical Association*, 100(469):310–321, 2005.
- [7] Christopher J Paciorek and Mark J Schervish. Spatial modelling using a new class of nonstationary covariance functions. *Environmetrics*, 17(5):483–506, 2006.
- [8] Thaís CO Fonseca and Mark FJ Steel. A general class of nonseparable space–time covariance models. *Environmetrics*, 22(2):224–242, 2011.
- [9] Moreno Bevilacqua, Carlo Gaetan, Jorge Mateu, and Emilio Porcu. Estimating space and space-time covariance functions for large data sets: a weighted composite likelihood approach. *Journal of the American Statistical Association*, 107(497):268–280, 2012.
- [10] Nan-Jung Hsu, Ya-Mei Chang, and Hsin-Cheng Huang. A group lasso approach for non-stationary spatial–temporal covariance estimation. *Environmetrics*, 23(1):12–23, 2012.
- [11] InKyung Choi, Bo Li, and Xiao Wang. Nonparametric estimation of spatial and space-time covariance function. *Journal of Agricultural, Biological, and Environmental Statistics*, 18(4):611–630, 2013.
- [12] Knut Solna and Paul Switzer. Time trend estimation for a geographic region. *Journal of the American Statistical Association*, 91(434):577–589, 1996.

- [13] Christopher K Wikle and Noel Cressie. A dimension-reduced approach to space-time kalman filtering. *Biometrika*, 86(4):815–829, 1999.
- [14] Hsin-Cheng Huang and Nan-Jung Hsu. Modeling transport effects on ground-level ozone using a non-stationary space–time model. *Environmetrics*, 15(3):251–268, 2004.
- [15] Ke Xu, Christopher K Wikle, and Neil I Fox. A kernel-based spatio-temporal dynamical model for nowcasting weather radar reflectivities. *Journal of the American Statistical Association*, 100(472):1133–1144, 2005.
- [16] Alan E Gelfand, Sudipto Banerjee, and Dani Gamerman. Spatial process modelling for univariate and multivariate dynamic spatial data. *Environmetrics*, 16(5):465–479, 2005.
- [17] Gardar Johannesson, Noel Cressie, and Hsin-Cheng Huang. Dynamic multi-resolution spatial models. *Environmental and Ecological Statistics*, 14(1):5–25, 2007.
- [18] Fabio Sigrist, Hans R Künsch, and Werner A Stahel. A dynamic nonstationary spatio-temporal model for short term prediction of precipitation. *The Annals of Applied Statistics*, 6(4):1452–1477, 2012.
- [19] Dan W Gladish and Christopher K Wikle. Physically motivated scale interaction parameterization in reduced rank quadratic nonlinear dynamic spatio-temporal models. *Environmetrics*, 25(4):230–244, 2014.
- [20] Robert Tibshirani. Regression shrinkage and selection via the lasso. *Journal of the Royal Statistical Society. Series B (Methodological)*, 58(1):267–288, 1996.
- [21] Lewis L Thurstone. Multiple factor analysis. *Psychological Review*, 38(5):406, 1931.
- [22] Rudolph Emil Kalman. A new approach to linear filtering and prediction problems. *Journal of Fluids Engineering*, 82(1):35–45, 1960.
- [23] Pierre Comon. Independent component analysis, a new concept? *Signal Processing*, 36(3):287–314, 1994.
- [24] Karl Pearson. Liii. on lines and planes of closest fit to systems of points in space. *The London, Edinburgh, and Dublin Philosophical Magazine and Journal of Science*, 2(11):559–572, 1901.
- [25] Ian Jolliffe. *Principal component analysis*. Wiley Online Library, 2002.
- [26] Harold Hotelling. Analysis of a complex of statistical variables into principal components. *Journal of Educational Psychology*, 24(6):417, 1933.

- [27] Kari Karhunen. Über lineare methoden in der wahrscheinlichkeitsrechnung. *Ann. Acad. Sci. Fennicae. Ser. A. I. Math.-Phys.*, 37:1–79, 1947.
- [28] Michel Loève. Fonctions aléatoires de second order. In Paul Lévy, editor, *Processus Stochastique et Movement Brownien*. Hermann, Paris, 1948.
- [29] Edward N Lorenz. Empirical orthogonal functions and statistical weather prediction. Scientific report no.1, Massachusetts Institute of Technology, Department of Meteorology, 1956. Statistical Forecasting Project.
- [30] George EP Box and George C Tiao. A canonical analysis of multiple time series. *Biometrika*, 64(2):355–365, 1977.
- [31] Peter CM Molenaar. A dynamic factor model for the analysis of multivariate time series. *Psychometrika*, 50(2):181–202, 1985.
- [32] Andrew D Back and Andreas S Weigend. A first application of independent component analysis to extracting structure from stock returns. *International Journal of Neural Systems*, 8(04):473–484, 1997.
- [33] Mario Forni, Marc Hallin, Marco Lippi, and Lucrezia Reichlin. The generalized dynamic-factor model: Identification and estimation. *Review of Economics and Statistics*, 82(4):540–554, 2000.
- [34] James H Stock and Mark W Watson. Forecasting using principal components from a large number of predictors. *Journal of the American Statistical Association*, 97(460):1167–1179, 2002.
- [35] David S Matteson and Ruey S Tsay. Dynamic orthogonal components for multivariate time series. *Journal of the American Statistical Association*, 106(496):1450–1463, 2011.
- [36] Zhaoran Wang, Fang Han, and Han Liu. Sparse principal component analysis for high dimensional multivariate time series. In *Proceedings of the Sixteenth International Conference on Artificial Intelligence and Statistics*, volume 31, pages 48–56, 2013.
- [37] Jinyuan Chang, Bin Guo, and Qiwei Yao. Segmenting multiple time series by contemporaneous linear transformation. *arXiv preprint arXiv:1410.2323*, 2014.
- [38] Mario Forni, Marc Hallin, Marco Lippi, and Paolo Zaffaroni. Dynamic factor models with infinite-dimensional factor spaces: One-sided representations. *Journal of Econometrics*, 185(2):359–371, 2015.

- [39] Michael Ghil, MR Allen, MD Dettinger, K Ide, D Kondrashov, ME Mann, Andrew W Robertson, A Saunders, Y Tian, F Varadi, and P Yiou. Advanced spectral methods for climatic time series. *Reviews of Geophysics*, 40(1):3–1–3–41, 2002.
- [40] David R Brillinger. *Time series: data analysis and theory*. Holden-Day, 1981.
- [41] Miguel Arevallilo Herráez, David R Burton, Michael J Lalor, and Munther A Gdeisat. Fast two-dimensional phase-unwrapping algorithm based on sorting by reliability following a noncontinuous path. *Applied Optics*, 41(35):7437–7444, 2002.
- [42] Joe H Ward Jr. Hierarchical grouping to optimize an objective function. *Journal of the American Statistical Association*, 58(301):236–244, 1963.
- [43] Eugenia Kalnay, Masao Kanamitsu, Robert Kistler, William Collins, Dennis Deaven, Lev Gandin, Mark Iredell, Suranjana Saha, Glenn White, and John Woollen. The ncep/ncar 40-year reanalysis project. *Bulletin of the American Meteorological Society*, 77(3):437–471, 1996.

A1 Computation details for examples

Rotating energy source examples. For applying phase-aligned spectral filtering (PASF) to the *rotating energy source* examples, the bandwidth of the Daniell kernel used for smoothing the raw periodogram is chosen to be 21. The threshold Δ is decided by the spectral gap in the pooled eigenvalues. The total number of selected eigenvectors is 80 for the low- and mid-noise cases and 38 for the high-noise case.

For PCA and ICA, we extract the first two components with highest energy, that is, the two components corresponding to the first two largest eigenvalues.

For SSA, the first 10 largest singular values are dominant in the low- and mid-noise level settings. In the high-noise setting, the gap appears between the eighth and ninth largest singular values. We divide the corresponding components into two groups by clustering them based on their weighted correlation and reconstruct the final two components from each group. The weighted correlation $\rho_w(\cdot, \cdot)$ is a measure of the degree of separability between two series and defined as

$$\rho_w(\zeta_t, \eta_t) = \frac{(\zeta_t, \eta_t)_w}{\|\zeta_t\|_w \|\eta_t\|_w},$$

where $\|\cdot\|_w = \sqrt{(\cdot, \cdot)_w}$, $(\zeta_t, \eta_t)_w = \sum_{k=1}^n w_k \zeta_k \eta_k$, $w_k = \min(k, n/2, n - k)$, and both of the two series ζ_t and η_t have a time length equal to n .

For PCA4TS, we choose the two groups whose corresponding components in the original space have largest variance.

Signal propagation examples. The bandwidth of the Daniell kernel for smoothing the raw periodogram is chosen to be 21. The total number of selected eigenvectors is 1000 and the dendrogram displays four clean clusters. The resulting components obtained from our algorithm show evident dynamics of four processes propagating on the grid area which perfectly correspond to the generated signals.

We extract the first four components for the PCA and ICA respectively. For SSA, we divide the first 50 components into four groups by clustering them based on their weighted correlation and reconstruct one new component from each group. For PCA4TS, we choose the four groups whose corresponding components in the original space have the largest variance.

Real data analysis: sea level pressure. The observations were first demeaned for each location before analysis. The bandwidth of the Daniell kernel for smoothing the periodogram was chosen to be 21. The total number of selected eigenvectors is 2000 and the resulting number of clusters is 2.

As in the simulation examples, we extract the first two components from PCA and ICA. We cluster the components from SSA into two groups based on their weighted correlation to obtain two final additive components. We select the first two components with the largest variance from PCA4TS.

A2 Connecting phase correlation with simple spatiotemporal dynamics

In this section we show that two common spatiotemporal dynamics can create phase correlation between their spectral densities at different frequencies.

A2.1 Signal Propagation

Assume that there are r independent real-valued signal processes $\{X_{1,t}, \dots, X_{r,t}\}$ propagating and the observed process $\mathbf{Z}_t = (Z_{s_1,t}, \dots, Z_{s_m,t})^\top \in \mathbb{R}^m$ satisfies

$$Z_{s_j,t} = \sum_{k=1}^r a_{jk} X_{k,t-t_{jk}},$$

where $a_{jk} > 0$ and the spectral density of $(X_{1,t}, X_{2,t}, \dots, X_{r,t})^\top$ is

$$f_{xx}(\omega) = \begin{pmatrix} \lambda_1(\omega) & & & \\ & \ddots & & \\ & & \ddots & \\ & & & \lambda_r(\omega) \end{pmatrix}.$$

Then the element of the spectral density of \mathbf{Z} in the j -th row and l -th column is given by

$$[f_{zz}(\omega)]_{j,l} = \sum_{k=1}^r a_{jk} a_{lk} e^{-2\pi i \omega (t_{jk} - t_{lk})} \lambda_k(\omega).$$

If we define

$$\begin{aligned} \mathbf{A}(\omega) &= [a_{jk} e^{-2\pi i \omega t_{jk}}]_{1 \leq j \leq m, 1 \leq k \leq r} \\ &= \begin{pmatrix} a_{11} e^{-2\pi i \omega t_{11}} & a_{12} e^{-2\pi i \omega t_{12}} & \dots & a_{1r} e^{-2\pi i \omega t_{1r}} \\ a_{21} e^{-2\pi i \omega t_{21}} & a_{22} e^{-2\pi i \omega t_{22}} & \dots & a_{2r} e^{-2\pi i \omega t_{2r}} \\ \vdots & \vdots & \dots & \vdots \\ a_{m1} e^{-2\pi i \omega t_{m1}} & a_{m2} e^{-2\pi i \omega t_{m2}} & \dots & a_{mr} e^{-2\pi i \omega t_{mr}} \end{pmatrix} \end{aligned}$$

then $f_{zz}(\omega) = \mathbf{A}(\omega) f_{xx}(\omega) \overline{\mathbf{A}(\omega)^\top}$. The phase of $\mathbf{A}(\omega)$ is $[-2\pi \omega t_{jk}]_{1 \leq j \leq m, 1 \leq k \leq r}$ which is a linear function of ω .

A2.2 Rotating Energy Source

Consider a mobile energy source defined by (c_t, E_t) where $c_t \in \mathbb{R}^2$ is the rotating trajectory and $E_t \in \mathbb{R}$ is the energy it carries at time t . Assume that c_t orbits around a center c_0 with uniform angular speed v_θ . That is,

$$c_t = c_0 + \begin{pmatrix} r \cos(\theta_0 + v_\theta t) \\ r \sin(\theta_0 + v_\theta t) \end{pmatrix}.$$

where θ_0 is the initial angle and r is the distance between c_0 and c_t .

Now consider the observation $z_{s,t}$ being the absorbed energy from the signal at location s and time t where $s \in \mathbb{R}^2$ can be written as

$$s = c_0 + \begin{pmatrix} r_s \cos \theta_s \\ r_s \sin \theta_s \end{pmatrix}.$$

Assume that $z_{s,t}$ is in the form of

$$z_{s,t} = E_t \cdot \kappa(\|s - c_t\|^2),$$

where $\kappa(\cdot)$ is a non-negative real-valued monotone decreasing function satisfying $\kappa(0) \leq 1$, and $\|s - c_t\|$ is the Euclidean distance between s and c_t , that is,

$$\begin{aligned} \|s - c_t\|^2 &= r^2 + r_s^2 - 2rr_s \cos(\theta_0 + v_\theta t - \theta_s) \\ &= r^2 + r_s^2 - 2rr_s \cos\left(v_\theta\left(t - \frac{\theta_s - \theta_0}{v_\theta}\right)\right). \end{aligned}$$

We assume $E_t = E_0$ for stationarity, that is, E_t does not change over time. Let

$$f_{s,t} = E_0 \cdot \kappa(r^2 + r_s^2 - 2rr_s \cos(v_\theta t))$$

and \mathcal{F}_s be the Fourier Transform of $f_{s,t}$. Then the Fourier Transform of $z_{s,t}$ is

$$\mathcal{F}_{z_s}(\omega) = F_s(\omega) \exp\left(-2\pi i \omega \frac{\theta_s - \theta_0}{v_\theta}\right)$$

Since $f_{s,t}$ is a symmetric function of t , \mathcal{F}_s is real. Therefore the modulus of \mathcal{F}_{z_s} is $|F_s(\omega)|$ and the phase

$$\text{Arg}(\mathcal{F}_{z_s}(\omega)) = \begin{cases} -2\pi\omega \frac{\theta_s - \theta_0}{v_\theta} & \text{if } F_s(\omega) \geq 0 \\ -2\pi\omega \frac{\theta_s - \theta_0}{v_\theta} + \pi & \text{if } F_s(\omega) < 0 \end{cases}$$

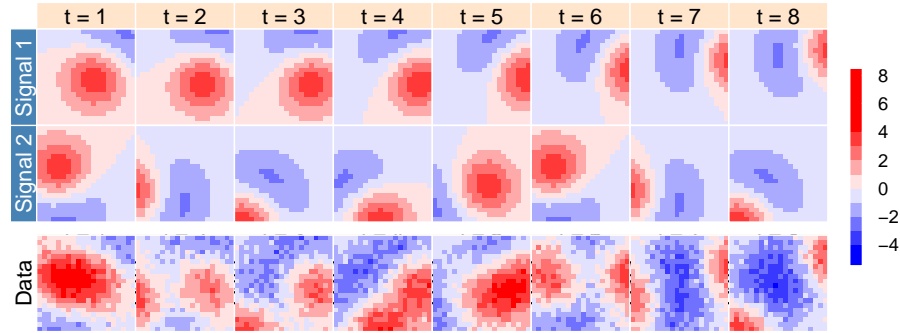
is a linear function of ω .

A3 Additional figures

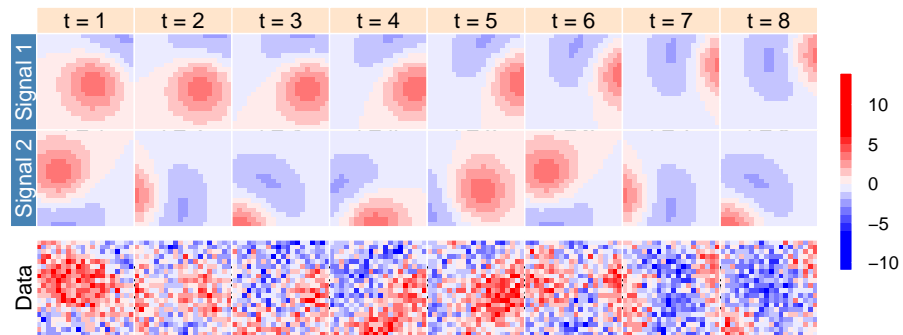
Table 1: Links to Animated Figures

URL	Description
http://goo.gl/LePZNs	two rotating energy sources, simulation example, low-noise level
http://goo.gl/tGld5F	two rotating energy sources, simulation example, mid-noise level
http://goo.gl/YB9HcW	two rotating energy sources, simulation example, high-noise level
http://goo.gl/JCpAjB	four propagating signals, simulation example
http://goo.gl/wiKEVt	sea level pressure, real data example

(a) Low-noise level: $\sigma_\varepsilon^2 = 0.16$



(b) Mid-noise level: $\sigma_\varepsilon^2 = 4$



(c) High-noise level: $\sigma_\varepsilon^2 = 16$

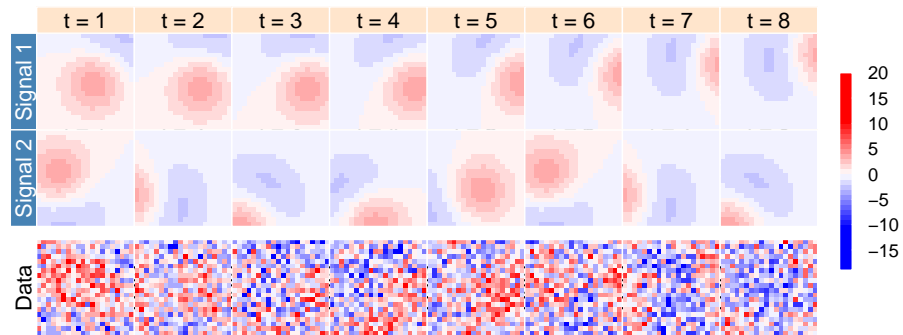


Figure A1: Level plots of the two rotating energy sources and observed data at selected time in the low-, mid- and high-noise level settings.

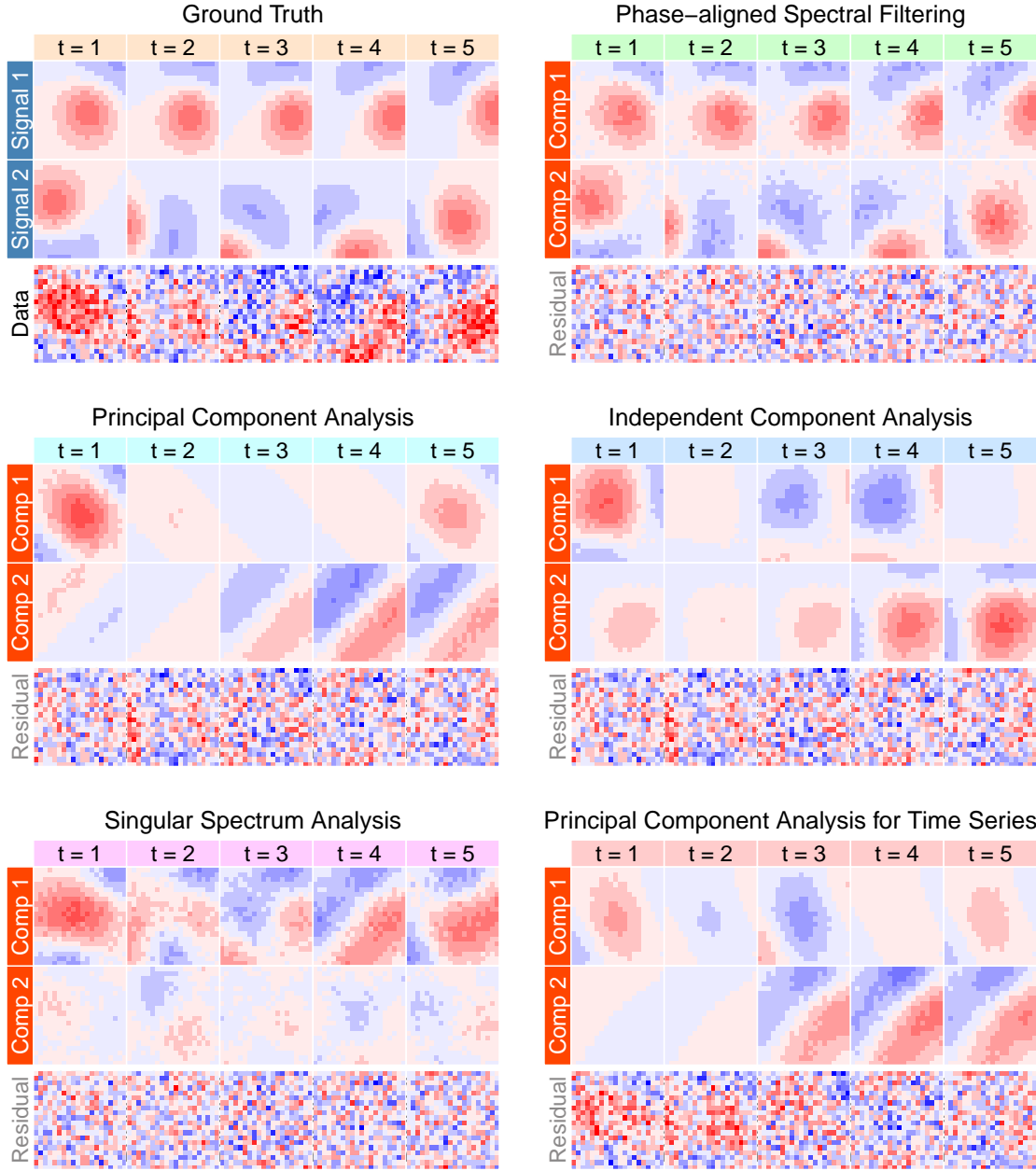


Figure A2: Decomposition results from different methods in the two-rotating-energy-source simulation in the mid-noise level setting with $\sigma_\epsilon^2 = 4$.

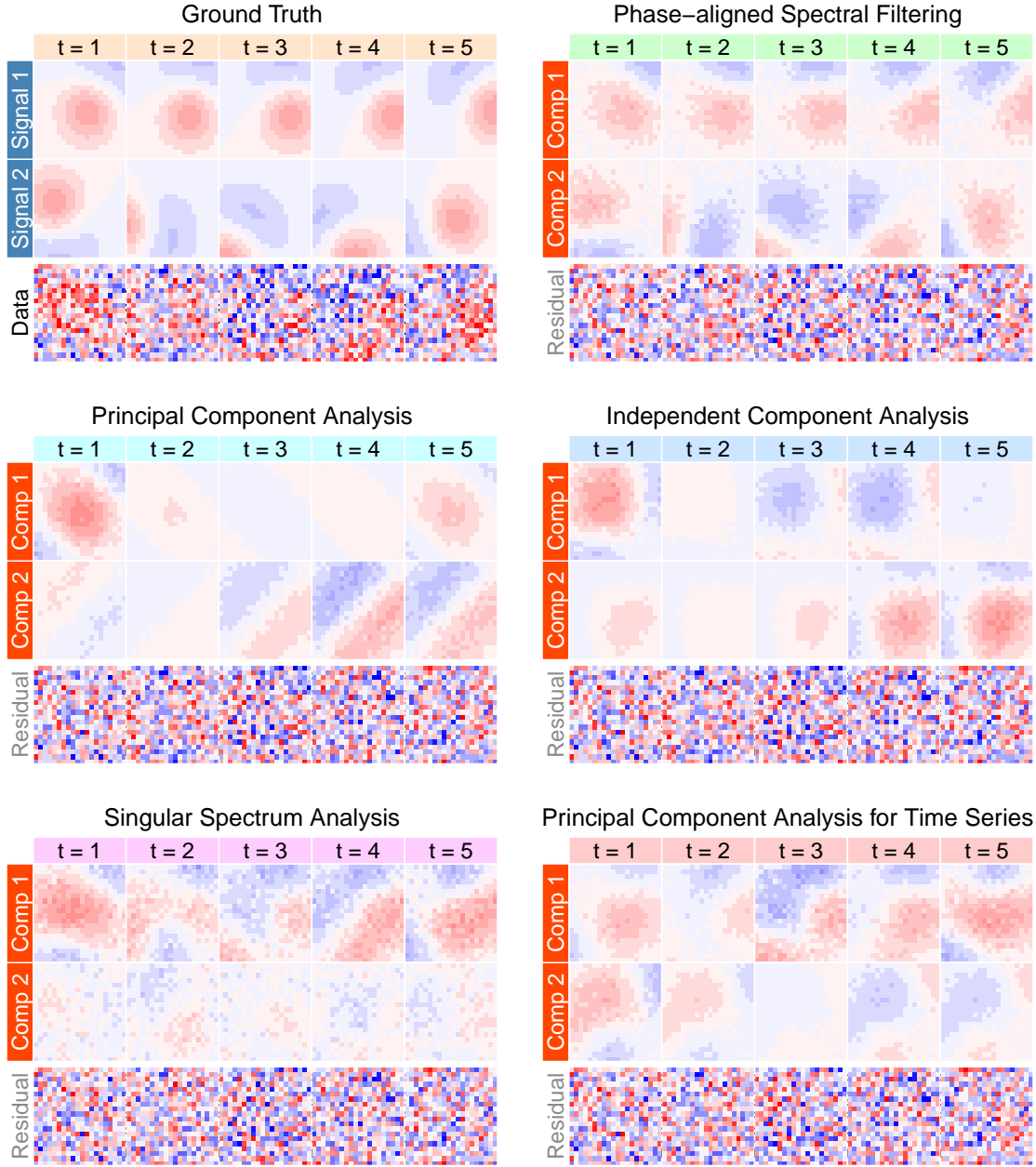


Figure A3: Decomposition results from different methods in the two-rotating-energy-source simulation in the high-noise level setting with $\sigma_\epsilon^2 = 16$.